Design Analysis and Capacitance Reduction of Hybrid Modular Multilevel Converters Under Boost AC Mode

Yaqian Zhang, *Member, IEEE*, Yi Zhang, *Member, IEEE*, Jianzhong Zhang, *Senior Member, IEEE*, Fujin Deng, *Senior Member, IEEE*, and Frede Blaabjerg, *Fellow, IEEE*

***Abstract*—This article offers an in-depth analysis of the hybrid modular multilevel converter (MMC) working steadily under boost ac mode and proposes an improved capacitance design approach reducing its overall capacitance without affecting the performance. This enables more cost-effective and space-efficient applications of hybrid MMC in distribution networks. First, considering the uneven energy distributions, an analytical model is established to estimate the nonlinear capacitor energy variations of the two different types of submodules in the hybrid MMC with higher simplicity and adaptability. It quantitatively reveals that different energy variations have inherently occurred between the two types of submodules in the hybrid MMC under boost ac mode. Second, by fully utilizing this characteristic, the submodule capacitances are designed separately to avoid unnecessary oversize and minimize the overall capacitance. Based on a comprehensive evaluation of the proposed design, the overall capacitance of the hybrid MMC can be reduced by at least 36% compared with the existing method. Moreover, the proposed design has much lower power losses when the same capacitance is fulfilled by full-bridge MMC. Finally, the effectiveness of the proposed method is validated both by simulations and experiments.**

***Index Terms*—Boost ac mode, capacitance design, energy variations, hybrid modular multilevel converter (MMC).**

I. Introduction

THANKS to the excellent modularity and scalability, modular multilevel converters (MMCs) are highly recommended for grid modernization, e.g., high-voltage direct current [1], [2]. However, the high costs and bulky volumes of the conventional MMC hinder their potential for wider applications, especially for medium-voltage distribution networks.

To explore whether the MMC has any untapped potential, a revisit of its fundamentals is necessary. As shown in Fig. 1, the MMC has two most typical submodules (SMs), namely the half-bridge SM (HBSM) and the full-bridge SM (FBSM). The systems composed of either type of SM are called HB-MMC and FB-MMC, respectively, whereas a mixture of the two SMs forms a hybrid MMC. In existing studies, the applications of the MMC are dominated by the HB-MMC and the buck ac mode operation, namely, the ac voltage amplitude does not exceed half of the dc voltage (i.e., $U_{\rm ac} \leq U_{\rm dc}/2$) [3], [4]. This working mode is inherently limited by the hardware of the HBSM, where ensuring $U_{\rm ac} \leq U_{\rm dc}/2$ can achieve a high-quality ac voltage without distortions [5]. In the following, the FB-MMC and hybrid MMC still follow the buck ac mode operation, where the inclusion of the FBSMs only considers dc fault protection [6]. However, the MMC with the integration of FBSMs can break through the buck ac mode and work under the boost ac mode, namely $U_{\rm ac} > U_{\rm dc}/2$ or the modulation index is larger than one [7], [8]. This feasible operating range has not been given sufficient discussion for a long time, but it has the potential to address some limitations and extend the application ranges of the MMC.

Some literature have already mentioned the great potential of the boost ac mode in the applications, such as distribution networks and power generation. Specifically, the boost ac mode allows the MMC to directly connect to the medium-voltage ac (MVAC) grid without bulky line frequency transformers (LFT), as shown in Fig. 2. The low-voltage dc (LVDC) terminals can be either various dc loads, i.e., electric vehicle (EV) charger and power-to-hydrogen, or dc sources, i.e., storage system [9], [10], [11], whose power integration into the MVAC networks are realized by the hybrid MMC-based system. The hybrid MMC is directly connected with the MVAC grid, and the medium-voltage dc (MVDC) side is cascaded by dc/dc converters, where the high-frequency transformers (HFT) or medium-frequency transformers (MFT) fulfill the isolation between the medium- and low-voltage sides. By the boost ac mode of the hybrid MMC, the MVDC voltage can be reduced so that the number of cascaded dc/dc converters is reduced to achieve lower cost and complexity of the overall grid-connected system. Nakanishi et al. [10] utilized the boost ac mode of the MMC to connect a 6.6 kV power grid to a microgrid system. By removing the LFT, the overall volume of the MMC is reduced by 90%. Meanwhile, Camurca et al. [11] proposed a new concept of using the boost ac mode of the MMC to form fast EV charging infrastructures,

Manuscript received 27 March 2023; revised 1 July 2023; accepted 22 August 2023. Date of publication 1 September 2023; date of current version 23 October 2023. This work was supported by the Science and Technology Projects of Jiangsu Province under Grant BE2022016. Recommended for publication by Associate Editor Tomislav Dragicevic. *(Corresponding authors: Jianzhong Zhang; Yi Zhang.)*

Yaqian Zhang, Jianzhong Zhang, and Fujin Deng are with the School of Electrical Engineering, Southeast University, Nanjing 210096, China (e-mail: yqzh@seu.edu.cn; jiz@seu.edu.cn; fdeng@seu.edu.cn).

Yi Zhang and Frede Blaabjerg are with the Department of Energy Technology, Aalborg University, 9220 Aalborg, Denmark (e-mail: yiz@ieee.org; fbl@energy.aau.dk).

Color versions of one or more figures in this article are available at https://doi.org/10.1109/TPEL.2023.3311046.

Digital Object Identifier 10.1109/TPEL.2023.3311046

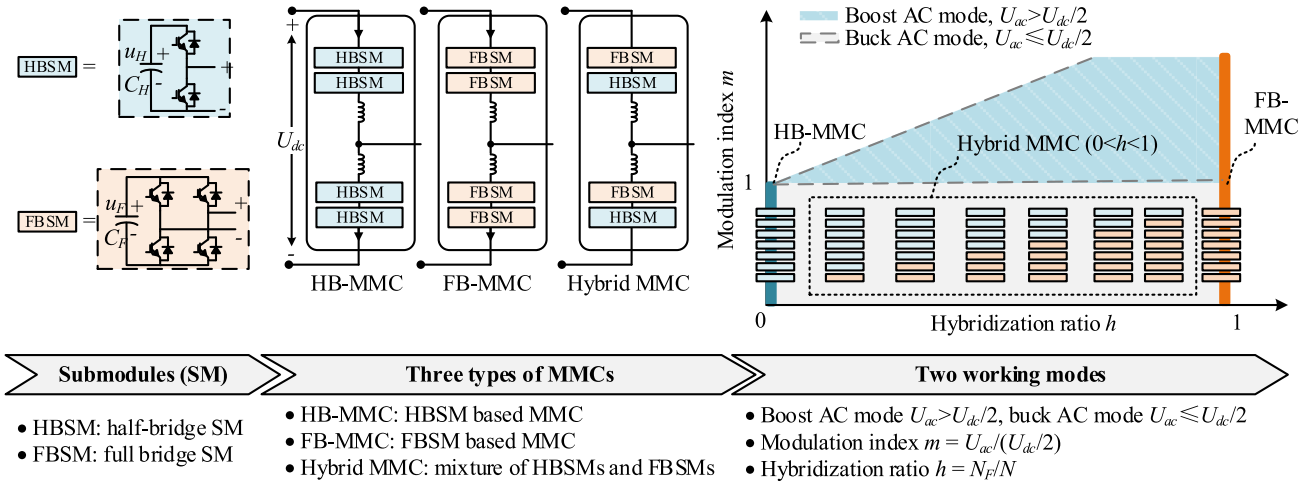

Fig. 1. Different working modes of three types of MMCs. The HB-MMC, FB-MMC, and hybrid MMC all can work under the buck ac mode. Only the hybrid MMC and FB-MMC are able to work under the boost ac mode. Hybridization ratio: Ratio of the number of FBSMs over the total number of SMs in an arm.

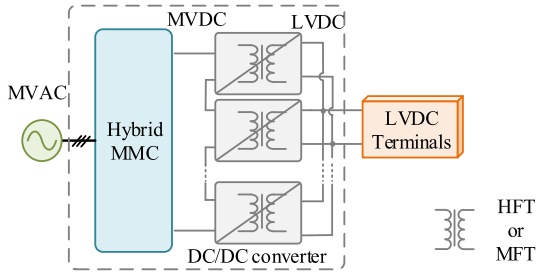

Fig. 2. Grid-connected system based on MMC under AC mode.

which enables the advantages of higher power density, higher reliability, and simpler structures. However, all aforementioned studies discuss the boost ac mode based on the FB-MMC only. The potential application of the hybrid MMC is not given enough attention.

Compared with FB-MMC, the hybrid MMC has more advantages to realize the boost ac mode, such as fewer FBSMs, lower costs, and lower power losses [12], [13], [14], [15]. However, due to the different voltage outputs of the HBSM and FBSM under the boost ac mode, their energy distributions have inherent differences and nonlinearity [16]. This limitation does not exist for the hybrid MMC working under the traditional buck ac mode because two types of SMs work identically. Whereas, when working under the boost ac mode, the FBSM must output both positive and negative voltage while the HBSM only outputs positive voltage. Neglecting this characteristic and directly applying the capacitor design methods developed from the traditional buck ac mode are prone to causing overdesign. Therefore, to better design the SM capacitance of the hybrid MMC under the boost ac mode, further investigations are necessary to fully understand the mechanism of this special working mode.

Basically, there are three intertwined problems worth noticing and to be solved. First, the hybridization ratio, which is the ratio of the number of FBSMs over the total number of SMs in an arm, affects the energy distributions between the two types of SMs. Currently, the hybridization ratio of the hybrid MMC is mainly determined by dc fault blocking requirement [8], [12]. However, considering the aforementioned distribution network and EV charging applications with relatively low dc voltages, a dc breaker is possibly a more efficient solution with lower power losses. This means that the dc fault blocking may not be a dominant factor to select the hybridization ratio. More factors, such as the required boost ac voltage and the voltage balancing between the HBSMs and the FBSMs, should be considered, which requires a revisit of the hybridization ratio of the hybrid MMC.

Second, the two different types of SMs in the hybrid MMC have uneven energy distribution under the boost ac mode. Specifically, the FBSMs must output both positive and negative voltage, whereas the HBSMs only output positive voltage [17]. This nonlinear operating mode makes it more difficult to estimate their energy variations. For simplification, Zhao et al. [18] assumed that all energy variations were carried by the FBSMs, however, this oversimplification caused an unexpected overdesign. To reduce the overdesign, several researchers assume that the energy variations are evenly distributed between HBSM and FBSM [12], [19], [20], which is correct for the traditional buck ac mode but essentially limited for the boost ac mode. As a result, their proposed methods seem to be errorless when applied to a hybrid MMC under low modulation index and high hybridization ratio, but the error becomes notable when the modulation index is high or the hybridization ratio is low. To address this challenge, Lin et al. [21] proposed a piecewise analysis, which dedicatedly divides the working period into four intervals. However, the given calculation process relies on the accurate location of a converging point, i.e., a specific time when the HBSM and FBSM capacitor voltages become equal. Considering the varied operating conditions, the accurate converging point positioning is substantially difficult and not clarified in [21] yet. Meanwhile, additional assumptions were made in [21] on the premise that the hybridization ratio is higher

than 0.667, which limits its applications in the entire hybridization ratio range. Besides, above all these studies of hybrid MMC, the HBSM capacitor energy variations are neglected without clear clarification. Therefore, considering the aforementioned limitations in terms of overdesign, narrowed applicable range, complex use, and incomplete analysis, further investigation is important to better estimate the SM capacitor energy variations of the hybrid MMC under the boost ac mode.

Third, due to the lack of theoretical understanding of the capacitor energy variations, the HBSM is often designed with identical capacitance to the FBSM for the hybrid MMC under the boost ac mode [12], [17], [18], [21]. This design principle is correct for the conventional buck ac mode, but it is questionable under the boost ac mode because the FBSM and the HBSM have inherently different energy variations. Therefore, based on the revealed characteristics of the hybrid MMC under boost ac mode, the capacitance design of the HBSM and FBSM capacitors requires reconsideration and improvements.

By addressing the aforementioned three challenges, this article proposes to utilize a hybrid MMC working under the boost ac mode to achieve a more compact and low-cost solution, which helps to extend the applications of the MMC. The contributions of this article are threefold.

1) A revisit of the hybridization ratio of the hybrid MMC is established, which more generally considers the three demands under the boost ac mode: the required negative output voltage, the dc fault blocking, and the voltage balancing.
2) An improved piecewise approach is proposed to estimate the nonlinear energy variations of the FBSM and HBSM capacitors, which are revealed to be inherently different when the hybrid MMC operates under the boost ac mode. Compared with the existing studies, the established analytical model acquires higher simplicity and accuracy without requiring the accurate coordinate of the converging point, and it is valid for a wider range of hybridization ratios.
3) By fully utilizing the inherently uneven energy variations, this article proposes to design the capacitance for the two types of SMs separately. Compared with the existing method, the proposed method reduces at least 36% of overall capacitance without degrading the performance. The proposed concept has a better efficiency as well.

II. Hybrid MMC Under Boost ac Mode

A. Basic Operation

Fig. 3 shows the configuration of the three-phase hybrid MMC. It has six arms, and each arm consists of an arm inductor L_s and N SMs, including N_H HBSMs and N_F FBSMs. C_H and C_F are their corresponding capacitance, and u_H and u_F are their corresponding capacitor voltage. The HBSM can only output two nonnegative voltage levels, i.e., 0 and $+U_C$, and the FBSM can output three bipolar voltage levels, i.e., 0, $+U_C$, and $-U_C$. U_C is the nominal voltage of both HBSM and FBSM capacitors.

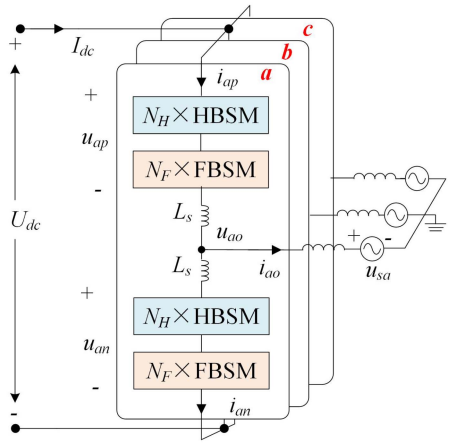

Fig. 3. Three-phase hybrid MMC. Each arm is cascaded by an arm inductor L_s, N_H HBSMs, and N_F FBSMs. (HBSM: Half-bridge SM. FBSM: Full-bridge SM.)

The ratio of the number of the FBSMs is defined as the hybridization ratio, which is given by

$$h = N_F/N. \tag{1}$$

This ratio plays a critical role in the hybrid MMC performance and will be further discussed in the next part.

Meanwhile, the modulation index is defined as

$$m = U_{\text{ac}}/(U_{dc}/2). \tag{2}$$

When $m \leq 1$, the MMC works under the buck ac mode, in which the FBSM and HBSM work identically. Instead, when the ac voltage amplitude is larger than half of the dc voltage with $U_{\text{ac}} > U_{\text{dc}}/2$, namely $m > 1$, the hybrid MMC works under the boost ac mode.

Considering the hybrid MMC working in an inverter mode, the upper arm voltage and current in phase a are expressed as

$$\begin{cases} u_{\text{ap}} = \frac{U_{\text{dc}}}{2} - U_{\text{ac}}\sin(\omega t) \\ i_{\text{ap}} = \frac{I_{\text{dc}}}{3} + \frac{I_{\text{ac}}}{2}\sin(\omega t + \varphi) \end{cases} \tag{3}$$

where u_{ap} and i_{ap} are the upper arm voltage and current, respectively. I_{dc} and I_{ac} are the dc current and ac current amplitude. U_{dc} and U_{ac} are the dc voltage and ac voltage amplitude. φ is the power factor angle. ω is the fundamental angular frequency.

The total number of SMs should support the peak arm voltage, which is expressed as

$$N = \max(u_{\text{ap}})/U_C = (U_{\text{ac}} + U_{\text{dc}}/2)/U_C. \tag{4}$$

The typical waveforms of the arm voltage and current of a hybrid MMC working under the boost ac mode are shown in Fig. 4. The FBSMs output negative voltage to extend the arm voltage into a negative part, which helps the hybrid MMC to have a higher ac voltage. The waveforms have four zero-crossing points $t_1(t_2)$ and $t_3(t_4)$, which mark the zero-crossing instants of the arm voltage and current in each cycle, respectively. They are

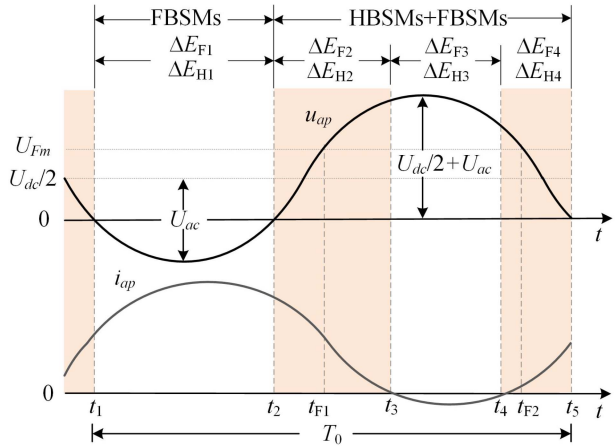

Fig. 4. Arm voltage and current of hybrid MMC under boost AC mode.

expressed as

$$\begin{cases} \omega t_1 = \arcsin\left(1/m\right) \\ \omega t_2 = \pi - \arcsin\left(1/m\right) \\ \omega t_3 = \arcsin\left(m \cdot \cos\varphi/2\right) - \varphi + \pi \\ \omega t_4 = 2\pi - \arcsin\left(m \cdot \cos\varphi/2\right) - \varphi. \end{cases} \tag{5}$$

With these zero-crossing points, the fundamental period can be divided into four intervals. The corresponding energy variations of the SMs are also divided into four intervals, where ΔE_{F1}, ΔE_{F2}, ΔE_{F3}, and ΔE_{F4} are for the FBSMs, whereas ΔE_{H1}, ΔE_{H2}, ΔE_{H3}, and ΔE_{H4} are for the HBSMs. The four intervals are introduced as follows.

1) [t_1, t_2]: The FBSMs output negative voltage to extend the arm voltage below zero. Here, the number of FBSMs must be able to support the maximum negative value of the arm voltage, which is

$$N_{F,\text{neg}} = \frac{\left|\min\left(u_{\text{ap}}\right)\right|}{U_C} = \frac{U_{\text{ac}} - U_{\text{dc}}/2}{U_C}. \tag{6}$$

Meanwhile, the HBSMs are all bypassed within $[t_1, t_2]$, and the FBSM capacitors are discharged. As a result, the FBSM capacitor voltage u_F and the HBSM capacitor voltage u_H have at $u_F < u_H$ at t_2.

2) [t_2, t_3]: Both the arm voltage and current are positive, so the SMs with lower voltages will be inserted in a higher priority to achieve the balancing of the capacitor voltages. Because $u_F < u_H$ at t_2, the FBSMs should be inserted and charged first at the beginning of $[t_2, t_3]$. When all the FBSMs are inserted achieving $U_{Fm} = U_C N_F$, a virtual time point t_{F1} is defined as $\omega t_{F1} = \pi - \arcsin(1/m - h(m+1)/m)$.

3) [t_3, t_4]: Due to the negative arm current within this period, the SMs with higher capacitor voltage should be inserted in higher priority for the capacitor voltage balancing.

4) [t_4, t_5]: This interval is similar to $[t_2, t_3]$ with $\omega t_{F2} = \arcsin(1/m - h(m+1)/m)$. The rest is not repeated.

In a summary, the FBSMs are working during the entire period, whereas the HBSMs can only work within $[t_2, t_5]$. This difference leads to uneven energy distributions between the two types of SMs and the nonlinearity of the capacitor energy variations.

B. Impact Factors of Hybridization Ratio

In existing work, the hybridization ratio of the MMC is only determined by the required dc fault blocking, which is typically a high ratio [18]. However, considering the application of the distribution network, e.g., the EV charging station [11], dc fault blocking might be not mandatory. The short dc cables have much lower possibilities of point-to-point short circuit faults. Moreover, the existing dc breaker might be more cost effective and efficient for the lower dc bus voltage in this case. Thus, a more general hybridization ratio is studied here. It considers not only the fault protection but also the impact of the required negative output of the arm voltage and the capacitor voltage balancing.

First, considering the conventional dc faults blocking, the corresponding hybridization ratio h_{dcf} is expressed as

$$h_{\text{dcf}} = \left(\sqrt{3}m\right)/\left(2\left(m+1\right)\right) \tag{7}$$

which is determined by the minimum required number of FBSMs for the dc fault blocking capability [18].

Next, under the boost ac mode of the hybrid MMC, a more critical requirement is to maintain the voltage balancing between the HBSM and the FBSM capacitors, which requires that the SM capacitor voltage varies stably around the nominal value. According to the imbalance mechanism of the capacitor energy in [6], the prerequisite of the voltage balancing should satisfy

$$2\int_{t_{F1}}^{t_3}\left(\left(u_{\text{ap}} - N_F U_C\right)\cdot i_{\text{ap}}\right)dt = -\int_{t_3}^{t_4}\left(\left(N - N_F\right)U_C \cdot i\right)dt \tag{8}$$

which ensures the zero net energy increase of the HBSM or FBSM capacitors during one fundamental period.

Submitting into (1), a hybridization ratio h_{bal} for voltage balancing is obtained as

$$2\int_{t_{F1}}^{t_3}\left(\left|\frac{1 - m\sin\left(\omega t\right)}{1+m} - h_{\text{bal}}\right|\cdot\left(m - 2\sin\left(\omega t\right)\right)\right)dt + \left(1 - h_{\text{bal}}\right)\int_{t_3}^{t_4}\left(m - 2\sin\left(\omega t\right)\right)dt = 0. \tag{9}$$

Last, combining (1) and (6), the corresponding hybridization ratio h_{neg} for the negative output capability is obtained as

$$h_{\text{neg}} = (m-1)/(m+1). \tag{10}$$

In a summary, the three hybridization ratios h_{dcf}, h_{bal}, and h_{neg} represent three different requirements of the hybrid MMC under the boost ac mode. Their relationship is shown in Fig. 5. Generally, the required negative voltage capability is the weakest constraint. When $m < 1.4$, the requirement of voltage balancing is almost identical to that of the negative output, but then increases rapidly under $m > 1.4$, even exceeding the requirement of dc fault blocking. In practice, the hybridization ratio should be

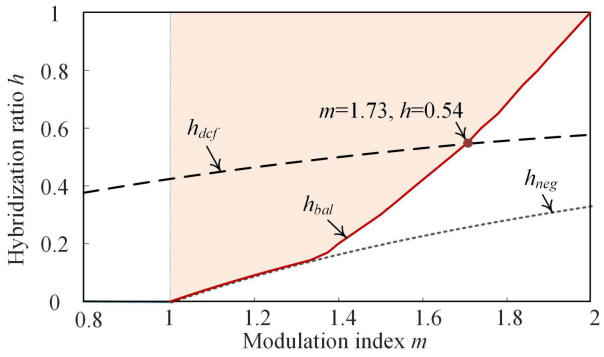

Fig. 5. Hybridization ratios for different operating requirements. (h_{neg}: negative voltage output. h_{dcf}: DC fault blocking. h_{bal}: voltage balancing.)

selected according to Fig. 5 based on different operating requirements. Compared with the existing literature only considering the hybridization ratio of $h \geq h_{\text{dcf}}$, the following analysis in this article will cover a wider range of hybridization ratios, i.e., $h \geq h_{\text{bal}}$.

III. Proposed Method to Estimate Capacitor Energy Variations by an Improved Piecewise Approach

Generally, the accurate calculation of energy variations over an entire fundamental period is a prerequisite for sizing capacitance, but it is complicated for the hybrid MMC working under the boost ac mode. Apart from the aforementioned uneven energy distributions and nonlinearity of the capacitor energy variations, an additional converging point exists for the hybrid MMC under the boost ac mode. As shown in Fig. 6, the converging point indicates the time that u_F and u_H become equal within a fundamental cycle, which is varied under different conditions and can be categorized into three different cases. To obtain accurate energy variations, Lin et al. [21] discussed the three different cases where each case is divided into four intervals. While this method is dedicated, there are still two remaining issues. First, the intensive categories under three different cases are complicated for engineering. Second, obtaining the accurate position of the converging point is substantially difficult, which is not only related to the operational conditions but also the sorting algorithm for balancing. Although the converging point is the prerequisite of determining the categories and calculating the energy variations in [21], its exact location has not been sufficiently elaborated.

Since it is difficult to calculate the unified energy variations over a whole fundamental cycle, this article takes the viewpoint that the maximum capacitor energy variations are enough to size the proper capacitance of the two types of SMs. Moreover, in contrast to obtaining the accurate location of the converging point, this article proposes to distinguish the three different cases simply and directly by comparing the derived energy variations. The entire method is named as an improved piecewise approach, which is introduced as follows.

A. Obtaining Maximum Energy Variation Instead of Calculating the Unified Energy Variation Across Entire Period

First, according to the four different time intervals and the corresponding energy fluctuations in Section II, the maximum energy variation of the FBSMs ΔE_F is expressed as

$$\Delta E_F = \max\left(\left|\Delta E_{F1}\right|, \quad \left|\Delta E_{F2}\right|, \quad \left|\Delta E_{F3}\right| \right) \tag{11}$$

where ΔE_{F4} is ignored since the maximum energy variation always has $|\Delta E_{F2}| \geq |\Delta E_{F4}|$ [21]. Similarly, the HBSMs have only one discharging interval $[t_3, t_4]$ in each fundamental cycle, which determines the maximum energy variation. Thus, the HBSM capacitor energy variation is expressed as

$$\Delta E_H = \max\left(\left|\Delta E_{H3}\right|\right). \tag{12}$$

By this way, the original problem of calculating the energy variations over a fundamental cycle is simplified into the calculation of four discrete energy variations, namely, ΔE_{F1}, ΔE_{F2}, ΔE_{F3}, and ΔE_{H3} and finding their maximum values.

Taking case 1 in Fig. 6(a) as an example. The FBSMs undertake all the negative arm voltage during $[t_1, t_2]$, while all the HBSMs are bypassed. Then, the energy variation is only distributed into FBSMs and ΔE_{F1} is expressed as

$$\Delta E_{F1} = \frac{1}{N_F}\int_{t_1}^{t_2} \left(u_{\text{ap}} \cdot i_{\text{ap}}\right) dt. \tag{13}$$

Next, the energy variations during $[t_2, t_3]$ are affected by the converging point t_c. In the existing method, a piecewise method is implemented to obtain the energy variations of $[t_2, t_c]$ and $[t_c, t_3]$, respectively. However, obtaining the accurate location of the t_c is substantially difficult. To address this issue, this article proposes to utilize the energy balancing feature to obtain ΔE_{F1} indirectly. Specifically, the FBSM capacitors must have zero energy increase during $[t_1, t_5]$ for a hybrid MMC with voltage balancing, the energy variation of the FBSMs during $[t_2, t_3]$ is thus obtained indirectly as

$$\Delta E_{F2} = -\Delta E_{F1} - \Delta E_{F3} - \Delta E_{F4}. \tag{14}$$

This method avoids the need for the precise calculation of t_c. Moreover, due to the capacitor voltages having $u_H = u_F$ after t_c, the energy variations of the FBSMs during $[t_3, t_5]$ can be easily obtained as

$$\Delta E_{F3} + \Delta E_{F4} = \frac{1}{N}\int_{t_3}^{t_5} \left(u_{\text{ap}} \cdot i_{\text{ap}}\right) dt. \tag{15}$$

Substituting (13) and (15) into (14), ΔE_{F2} is thus derived as

$$\Delta E_{F2} = -\frac{1}{N}\int_{t_1}^{t_2} \left(u_{\text{ap}} i_{\text{ap}}\right) dt - \frac{1}{N}\int_{t_3}^{t_5} \left(u_{\text{ap}} i_{\text{ap}}\right) dt. \tag{16}$$

In addition, the arm energy variations are evenly distributed among each SM during $[t_3, t_4]$. The energy variations of the HBSM and FBSM capacitors are thus given by

$$\Delta E_{F3} = \Delta E_{H3} = \frac{1}{N}\int_{t_3}^{t_4} \left(u_{\text{ap}} i_{\text{ap}}\right) dt. \tag{17}$$

By this method, the four required energy variations of case 1 are obtained. The required estimations of cases 2 and 3 can

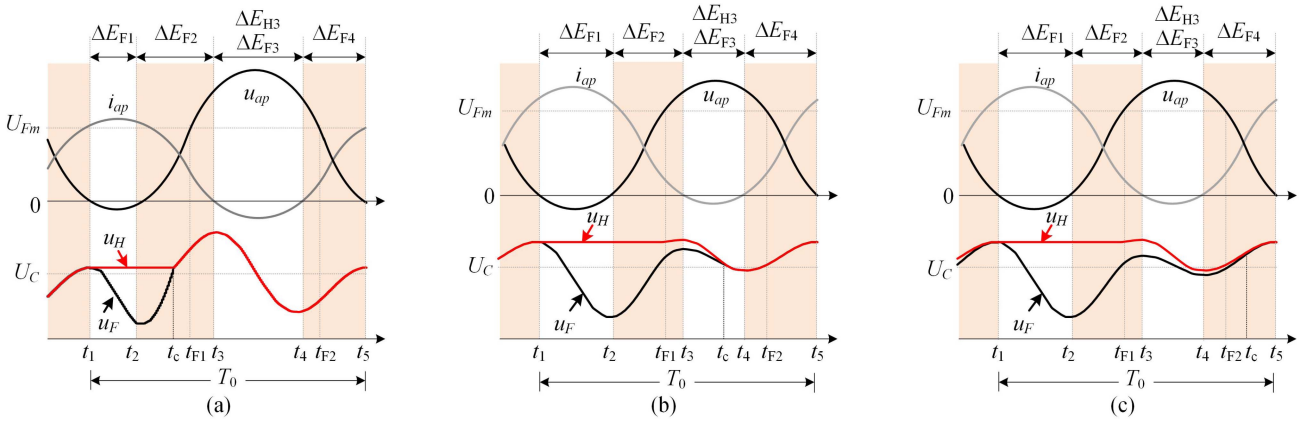

Fig. 6. Three cases with different locations of the converging point t_c. (a) Case 1: $t_2 < t_c \leq t_3$. (b) Case 2: $t_3 < t_c \leq t_4$. (c) Case 3: $t_4 < t_c \leq t_5$. u_H and u_F are the HBSM and FBSM capacitor voltages, respectively. Converging point t_c is the instant where u_H and u_F become equal.

TABLE I
SM CAPACITOR ENERGY VARIATIONS WITHIN FOUR INTERVALS IN DIFFERENT CASES: CASE 1, CASE 2, AND CASE 3

	Case 1	Case 2	Case 3
ΔE_{F1}	$\frac{\int_{t_1}^{t_2}(u_{\rm ap}\, i_{\rm ap})dt}{N_F}$	$\frac{\int_{t_1}^{t_2}(u_{\rm ap}\, i_{\rm ap})dt}{N_F}$	$\frac{\int_{t_1}^{t_2}(u_{\rm ap}\, i_{\rm ap})dt}{N_F}$
ΔE_{F2}	$-\frac{\int_{t_1}^{t_2}(u_{\rm ap}\, i_{\rm ap})dt}{N} - \frac{\int_{t_3}^{t_5}(u_{\rm ap}\, i_{\rm ap})dt}{N}$	$\frac{\int_{t_2}^{t_{F1}}(u_{\rm ap}\, i_{\rm ap})dt}{N_F} + \int_{t_{F1}}^{t_3}(U_C i_{\rm ap})\,dt$	$\frac{\int_{t_2}^{t_{F1}}(u_{\rm ap}\, i_{\rm ap})dt}{N_F} + \int_{t_{F1}}^{t_3}(U_C i_{\rm ap})\,dt$
ΔE_{F3}	$\frac{\int_{t_3}^{t_4}(u_{\rm ap}\, i_{\rm ap})dt}{N}$	$-\frac{\int_{t_1}^{t_{F1}}(u_{\rm ap}\, i_{\rm ap})dt}{N} - \frac{\int_{t_4}^{t_5}(u_{\rm ap}\, i_{\rm ap})dt}{N} - \int_{t_{F1}}^{t_3}(U_C i_{\rm ap})\,dt$	$\frac{\int_{t_3}^{t_4}((u_{\rm ap}-U_C N_H) i_{\rm ap})dt}{N_F}$
ΔE_{H3}	$\frac{\int_{t_3}^{t_4}(u_{\rm ap}\, i_{\rm ap})dt}{N}$	$-\frac{\int_{t_4}^{t_5}(u_{\rm ap}\, i_{\rm ap})dt}{N} - \frac{\int_{t_{F1}}^{t_3}((u_{\rm ap}-U_{Fm}) i_{\rm ap})dt}{N_H}$	$\int_{t_3}^{t_4}(U_C i_{\rm ap})\,dt$

be analyzed similarly. Finally, the results of all three cases are summarized and listed in Table I. Notably, the accurate position of t_c is not required in Table I to derive the energy variations accurately, which significantly simplifies the calculation process.

B. Determine Different Cases by Simply Comparing Three Estimated ΔE_{H3}

Although the aforementioned analysis relieves the need of obtaining the exact location of the converging point, determining its interval is still necessary to distinguish the three cases in which the hybrid MMC is operating. As listed in Table I, the calculation of ΔE_{H3} is different in the three cases. This is caused by the different locating intervals of the converging point. Therefore, this article proposes a simple method of comparing the three calculated ΔE_{H3} to decide the case. To describe them clearly, the three expressions of ΔE_{H3} in the three cases are denoted as $\Delta E_{H3,\text{case 1}}$, $\Delta E_{H3,\text{case 2}}$, and $\Delta E_{H3,\text{case 3}}$, respectively.

For case 1, the energy variations are evenly distributed between HBSMs and FBSMs at the interval of $[t_3, t_4]$, $\Delta E_{H3,\text{case 1}}$ is thus expressed as (17). Whereas, the HBSMs are inserted in a higher priority in case 2 or 3 due to the negative arm current and $u_F < u_H$. When wrongly applying $\Delta E_{H3,\text{case 1}}$ to case 2 or 3, the obtained energy variations of the HBSMs are underestimated, which are described as

$$\begin{cases} \text{Case 2}: & |\Delta \text{E}_{\text{H3,case 1}}| \leq |\Delta \text{E}_{\text{H3,case 2}}| \\ \text{Case 3}: & |\Delta E_{H3,\text{case 1}}| \leq |\Delta E_{H3,\text{case 3}}|\,. \end{cases} \tag{18}$$

Similarly, $\Delta E_{H3,\text{case 2}}$ is only valid for case 2. Since the converging point makes it difficult to directly calculate the energy variations at $[t_3, t_4]$ in case 2, the value of ΔE_{H3} is obtained indirectly according to energy balancing, which is

$$\Delta E_{H3,\text{case 2}} = -\Delta E_{H2} - \Delta E_{H4}. \tag{19}$$

When wrongly applying $\Delta E_{H3,\text{case 2}}$ to case 1, the value of ΔE_{H2} in (19) would be underestimated, leading to the underestimation of $|\Delta E_{H3}|$. This is because the HBSMs are charged less during $[t_2, t_3]$ in case 2, than in case 1. Similarly, the value of ΔE_{H4} would be overestimated when using $\Delta E_{H3,\text{case 2}}$ in case 3, leading to the overestimation of $|\Delta E_{H3}|$. Therefore, the relationships are given as

$$\begin{cases} \text{Case 1}: & |\Delta \text{E}_{\text{H3,case 2}}| \leq |\Delta \text{E}_{\text{H3,case 1}}| \\ \text{Case 3}: & |\Delta E_{H3,\text{case 3}}| \leq |\Delta E_{H3,\text{case 2}}|. \end{cases} \tag{20}$$

In case 3, the HBSMs are always discharged in higher priority at $[t_3, t_4]$. When wrongly applying $\Delta E_{H3,\text{case 3}}$ to case 1 or 2, the HBSM capacitor energy variations would be overestimated, which is denoted as

$$\begin{cases} \text{Case 1}: & |\Delta \text{E}_{\text{H3,case 1}}| \leq |\Delta \text{E}_{\text{H3,case 3}}| \\ \text{Case 2}: & |\Delta E_{H3,\text{case 2}}| \leq |\Delta E_{H3,\text{case 3}}|. \end{cases} \tag{21}$$

In summary, the validity of the aforementioned $\Delta E_{H3,\text{case 1}}$, $\Delta E_{H3,\text{case 2}}$, and $\Delta E_{H3,\text{case 3}}$ in Table I has their respective prerequisites. Wrongly applying the three expressions will cause either overestimation or underestimation of the HBSM capacitor energy variations. Combining (18), (20), and (21), the following

TABLE II
SPECIFICATIONS AND PARAMETERS OF THE STUDIED HYBRID MMC

Parameters and symbols	Values and units
Nominal active power S	10 MVA
AC output voltage U_{ac}	28 kV
Nominal SM voltage U_C	2 kV
Arm inductance L_s	5 mH

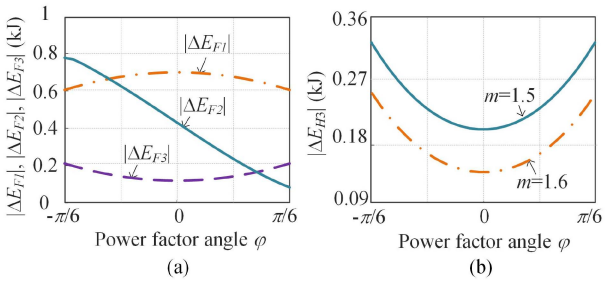

Fig. 7. Influence of power factor angle on the obtained energy variations. (a) FBSM capacitors. (b) HBSM capacitors ($h = 0.5$).

criterion is derived to distinguish the three cases:

$$\begin{cases} \text{Case 1}: & |\Delta \mathrm{E}_{\mathrm{H3,case\ 2}}| \le |\Delta \mathrm{E}_{\mathrm{H3,case\ 1}}| \le |\Delta \mathrm{E}_{\mathrm{H3,case\ 3}}| \\ \text{Case 2}: & |\Delta E_{H3,\text{case 1}}| \le |\Delta E_{H3,\text{case 2}}| \le |\Delta E_{H3,\text{case 3}}| \\ \text{Case 3}: & |\Delta E_{H3,\text{case 1}}| \le |\Delta E_{H3,\text{case 3}}| \le |\Delta E_{H3,\text{case 2}}|. \end{cases} \tag{22}$$

Without knowing the exact location of the converging point, the three different cases can be determined by simply comparing the three expressions.

C. Maximum Energy Variations Estimated by Proposed Method and Simulation Verification

Based on the parameters listed in Table II, Fig. 7 illustrates the influence of the power factor on the piecewise energy variations, where the absolute value is used. It shows that the maximum values of $|\Delta E_{F1}|$, $|\Delta E_{F2}|$, $|\Delta E_{F3}|$, and $|\Delta E_{H3}|$ occur when $\varphi = 0$, $\varphi = -\pi/6$, $\varphi = \pm\pi/6$, and $\varphi = \pm\pi/6$, respectively. Finally, the piecewise approach in (11) and (12) can be further given as

$$\Delta E_F = \max \begin{pmatrix} |\Delta E_{F1}|\,(\varphi = 0)\,, \\ |\Delta E_{F2}|\,(\varphi = -\varphi_m)\,, \\ |\Delta E_{F3}|\,(\varphi = \pm\varphi_m) \end{pmatrix} \tag{23}$$

$$\Delta E_H = |\Delta E_{H3}|\,(\varphi = \pm\varphi_m) \tag{24}$$

where φ_m denotes the maximum power factor angle and is set as $\pi/6$ in this article.

So far, the analytical model of the energy variations is established for both the HBSM and FBSM capacitors in the hybrid MMC under the boost ac mode, where the uneven energy distributions are fully considered under an extensive range of modulation indexes and hybridization ratios. This lays the theoretical foundation for further capacitance design.

Furthermore, Fig. 8 reveals the energy variations of the HBSM and FBSM capacitors under different modulation indexes and hybridization ratios. First, the simulated and calculated energy

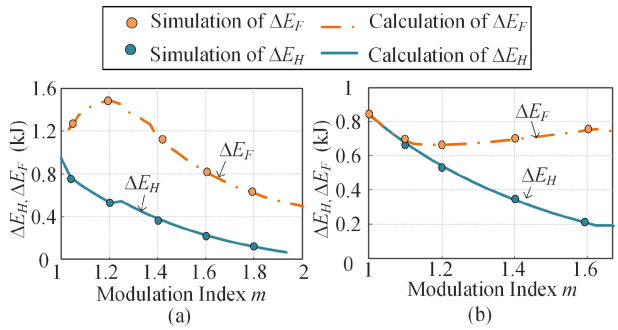

Fig. 8. Simulation verification of the obtained maximum energy variations by the proposed method. (a) $h = h_{\text{bal}}$, which is the minimum hybridization ratio to achieve voltage balancing and (b) $h = 0.5$. The energy variation of the FBSM capacitor is inherently higher than that of the HBSM.

variations match well for both the HBSM and FBSM, which verifies the proposed method. Second, the energy variations of the HBSM and FBSM capacitors have inherent deviations. As shown in Fig. 8(a), when the hybridization ratio is selected as $h = h_{\text{bal}}$, the maximum energy variation of the FBSMs ΔE_F is multiple times higher than that of HBSMs ΔE_H. Meanwhile, when the hybridization ratio is fixed at $h = 0.5$, the difference between the HBSM and FBSM becomes larger with the increase of the modulation index. These inherent energy differences between the two types of SMs are ignored or not fully exploited in the existing methods [18], [21], but this article will utilize this characteristic to further reduce the capacitance, which is discussed in the next section.

IV. Reduce Capacitance Based on Inherent Difference of Energy Variations and Evaluate Benefits

In contrast to the existing method ignoring the different energy variations of the two types of SMs, this article proposes to fully utilize this inherent characteristic to reduce the requirement of the capacitance in the hybrid MMC. A comprehensive evaluation is also provided to quantify the benefits of the proposed method.

A. Capacitance Design Considering the Inherently Different Energy Variations

According to [22], the design of the SM capacitance of the MMC follows the below expression, that is

$$C_{\text{SM}} = \frac{\Delta E_{\text{SM}}}{\varepsilon U_C^2} \tag{25}$$

where C_{SM} and ΔE_{SM} are the required capacitance and the energy variation of the SM, respectively. ε is the voltage ripple coefficient that is often around 10%. In the existing method, the different energy variations of HBSMs and FBSMs are ignored. ΔE_{SM} is determined by the maximum energy variation, that is ΔE_F. The HBSM capacitance is sized to be identical to the FBSM.

In this article, the established model of the energy variations reveals an inherent difference between the FBSM and HBSM. The existing efforts without considering this inherent characteristic will lead to an overdesign. Therefore, this article proposed

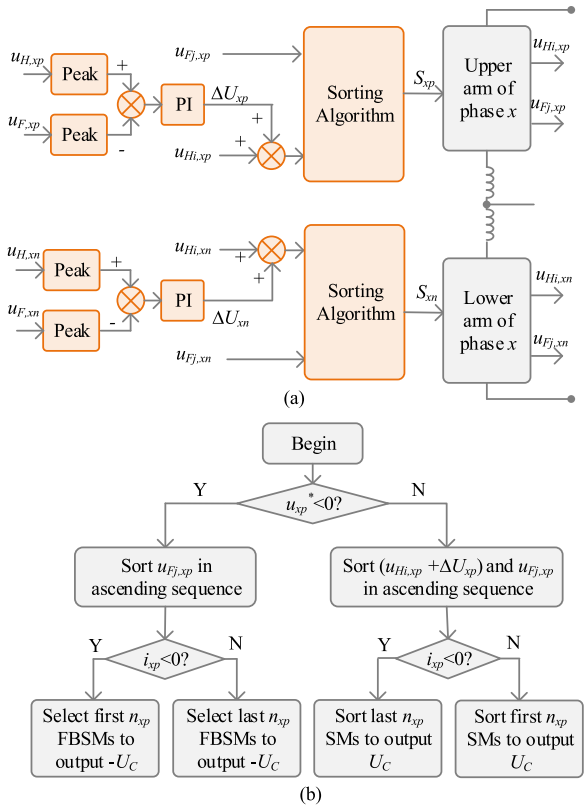

Fig. 9. Sorting algorithm based on peak voltage balancing control of SM capacitors. (a) Peak voltage balancing control of SM capacitors. (b) Sorting algorithm.

to size the capacitance of the two types of SM independently, which is given by

$$\begin{cases} C_H = \frac{\Delta E_H}{\varepsilon U_C^2} \\ C_F = \frac{\Delta E_F}{\varepsilon U_C^2} \end{cases} \tag{26}$$

where C_H and C_F are the capacitance of the HBSM and FBSM capacitors, respectively. The estimation of ΔE_H and ΔE_F is analyzed in detail in Section III. The benefits of this proposed capacitance design method are evaluated below.

B. Control of Hybrid MMC With Proposed Capacitance Design

The control of the hybrid MMC with the proposed capacitance design is mainly composed of the following several parts. The active/reactive power control, phase energy balancing control, arm energy balancing control, and circulating current control are similar to that of HB-MMC [1], [23], [24]. In terms of the modulation approach, the particular carrier phase-shift modulation was proposed in [25] for the medium-voltage hybrid MMC under boost ac mode.

Moreover, the sorting algorithm of the hybrid MMC in this article, is conducted based on the peak voltage balancing approach in [12], as shown in Fig. 9. x indicates the phase x, and i, j indicate the numberings of the HBSMs and FBSMs in each arm, respectively. In Fig. 9(a), the peak value of $u_{H,xp}$ and $u_{F,xp}$ are collected and compared to maintain the peak voltage balancing of the HBSM and FBSM capacitors, where the difference is input into a PI controller to get the voltage deviation ΔU_{xp}. Finally, the voltage ($u_{Hi,xp}$ +ΔU_{xp}) and $u_{Fj,xp}$ are used in the sorting algorithm in Fig. 9(b). In this way, the voltage of the HBSM capacitors have the same peak voltage to the FBSM capacitors. Fig. 9(b) presents the principle of the sorting algorithm. Only the FBSM capacitor voltage $u_{Fj,xp}$ needs to be sorted under the negative arm voltage of $u^*_{xp} < 0$, and all the SM capacitor voltage, ($u_{Hi,xp}$ +ΔU_{xp}) and $u_{Fj,xp}$, should be sorted simultaneously under the nonnegative arm voltage of $u^*_{xp} \geq 0$. The SMs with lower voltage should be charged in higher priority and discharged in lower priority, and the SMs with higher voltage should be discharged in higher priority and charged in lower priority.

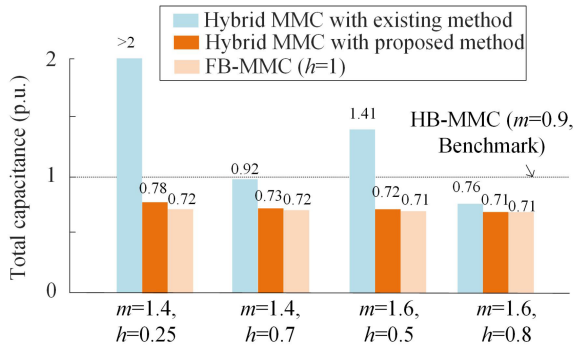

Fig. 10. Capacitance comparison of different MMCs under different modulation indexes and hybridization ratios. The total capacitance of the HB-MMC is seen as the benchmark (1 p.u.).

C. Benefits Evaluation of Proposed Capacitance Design Method

The benefits of the proposed design method are quantitatively evaluated based on the parameter listed in Table II. The case study aims to design a 10 MVA system where the ac voltage amplitude is 28 kV (line-to-line ac voltage is 35 kV). The capacitor volume, power losses, voltage balancing, and active/reactive capabilities are evaluated comprehensively.

1) Capacitor Volume: The overall capacitance is evaluated in Fig. 10, where the total capacitance of the HB-MMC is set as the benchmark [1 per unit (p.u.)] and the rest of the cases are normalized. First, ignoring the inherently different energy variations between the HBSM and FBSM in the hybrid MMC, the existing method of the hybrid MMC in [18] causes severe overdesign of the HBSM and FBSM capacitances due to the oversimplified calculation, especially for the condition with a low hybridization ratio ($h \leq 0.5$). It reveals that the existing design method does not fully unlock the benefits of the hybrid MMC working under the boost ac mode. On the contrary, the established model in this article reveals the inherent differences between the two types of SMs in the hybrid MMC. Then, by fully utilizing the characteristic of different energy variations and designing the HBSM and FBSM capacitance separately, the total capacitance can be reduced by around 50% compared with

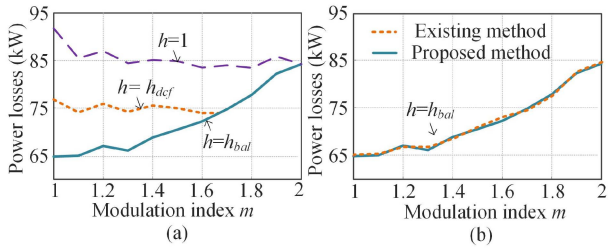

Fig. 11. Comparison of power losses under (a) different hybridization ratios and (b) different capacitance design methods.

the existing method and by 28% compared with the benchmark. Meanwhile, in the FB-MMC, all the SMs can generate negative output voltage and the required capacitance is the minimum. However, when the modulation index is high (i.e., $m = 1.6$), the hybrid MMC with $h = 0.5$ can achieve a similar capacitance reduction as the FB-MMC. Since only half of the SMs are FBSMs with $h = 0.5$, the hybrid MMC is expected to have better efficiency and lower hardware costs, which will be evaluated in the following.

2) Power Losses: The power losses are compared based on simulation with the IGBT FF450R33T3E3, and the estimation method refers to [26], [27]. As shown in Fig. 11(a), the comparison is carried based on three different hybridization ratios, i.e., $h = 1$, $h = h_{\text{dcf}}$, and $h = h_{\text{bal}}$. When $h = 1$, it is essentially an FB-MMC and the power losses are the largest. By reducing the hybridization ratio to $h = h_{\text{bal}}$, the hybrid MMC working under the boost ac mode can reduce power losses around 15%–25% compared with the FB-MMC. Meanwhile, as shown in Fig. 11(b), the proposed capacitance design considering the inherently different energy variations does not affect the power losses, although the existing method causes overdesign of the capacitance.

3) Voltage Balancing: Since the proposed method leads to different capacitances for the HBSMs and FBSMs of the hybrid MMC, the voltage balancing needs further confirmation. The simulation results are provided in Fig. 12 to verify that the proposed method does not affect the voltage balancing. As shown in Fig. 12(a), although both the HBSMs and FBSMs have identical capacitance, the capacitor voltage imbalance occurs due to the insufficient hybridization ratio ($h = 0.39$), which is less than the requirement of $h \geq 0.41$. As the hybridization ratio increases to 0.435 in Fig. 12(b), the voltage balancing of the HBSM and FBSMs is achieved. Also, due to the inherently different energy variations between them, the capacitor voltage ripple of the HBSM is obviously less than that of the FBSM. Based on the proposed method, different capacitances are selected for the two types of SMs as $C_F = 2.3$ mF and $C_H = 0.53$ mF, which can also achieve voltage balancing well, as shown in Fig. 12(c). The reduced HBSM capacitance enlarges the corresponding voltage ripple but is still within a safe margin, which improves the utilization of the capacitor.

4) P/Q Capability: This article discusses the operating range with full power within $[-\pi/6, \pi/6]$ but it can be extended to the full range. The energy variations of the HBSM and the FBSM under different power factor angles are shown in Fig. 13. The solid

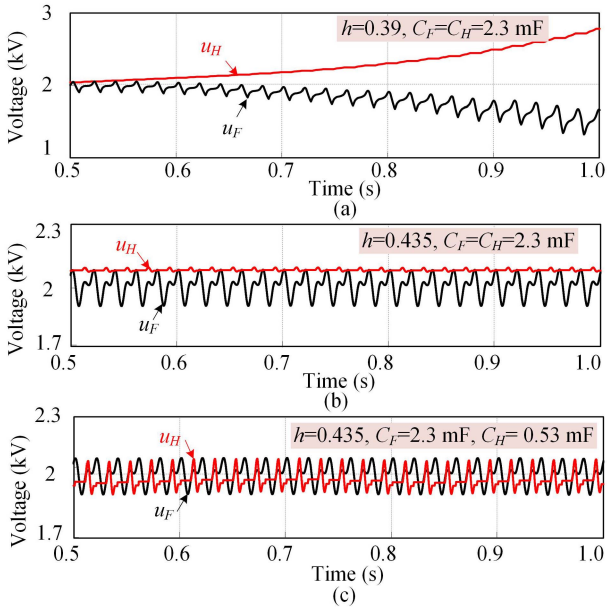

Fig. 12. Influence of the voltage balancing. (a) Identical capacitances of both HBSM and FBSM under $h = 0.39$. (b) Identical capacitances of both HBSM and FBSM under $h = 0.435$. (c) Proposed method with separate capacitance.

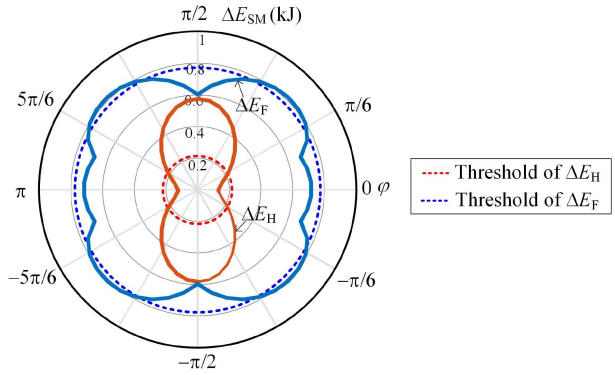

Fig. 13. Capacitor energy variations under different power factors. The solid lines indicate the full power, whereas the dash lines indicate the maximum energy variations of $\varphi \in [-\pi/6, \pi/6]$.

lines indicate the energy variations under the full power, whereas the dash lines are the thresholds within the range of $[-\pi/6, \pi/6]$. The value of ΔE_H under $\varphi = \pm\pi/2$ is about three times of that under $\varphi = \pm\pi/6$. Operating with full power at $\varphi = \pm\pi/2$ will lead to a large capacitance requirement. Thus, a possible way to work under $\varphi = \pm\pi/2$ is to limit the reactive power below $Q = 0.35$ p.u., which still remains within 10% voltage ripple of the HBSM capacitor. It also reveals that the hybrid MMC with the boost ac mode is more suitable for the applications with a high power factor, such as the aforementioned EV charging stations, renewable hydrogen production, and data center.

V. Simulation and Experimental Verification

A. Simulations

The MATLAB/Simulink simulations of a three-phase hybrid MMC are carried out to verify the proposed design approach,

TABLE III
SIMULATION PARAMETERS OF HYBRID MMC

Parameters and symbols	Values and units
Number of SMs N	23
Number of HBSMs N_H	11
Number of FBSMs N_F	12
DC bus voltage $U_{\rm dc}$	35 kV
HBSM capacitance C_H	1.92 mF
FBSM capacitance C_F	0.53 mF

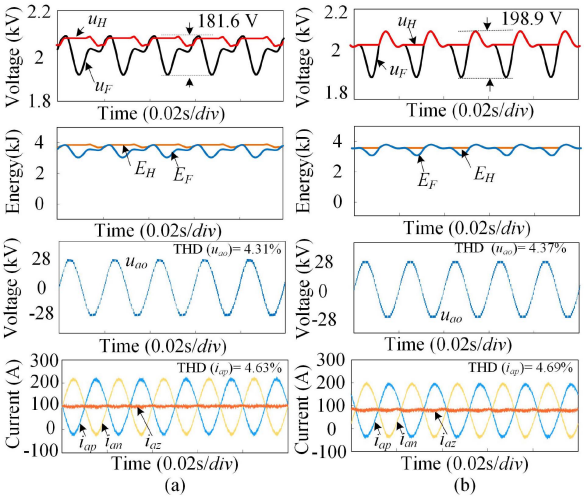

Fig. 14. Simulation result of hybrid MMC with $C_F = C_H$ =1.92 mF. (a) $\varphi = 0$, (b) $\varphi = -\pi/6$. The voltage ripple of the FBSM capacitor is much higher than that of the HBSM capacitor. (Top to Bottom: SM capacitor voltage, SM capacitor energy, AC output voltage, arm currents, and circulating current.)

with the parameters listed in Tables II and III. Fig. 14 shows that the HBSM and the FBSM of the hybrid MMC have identical capacitance, i.e., $C_F = C_H = 1.92$ mF. In the two cases of $\varphi = 0$ and $\varphi = -\pi/6$, the maximum voltage ripple of the FBSM capacitor is within 200 V (around 10% of the nominal capacitor voltage). Whereas, the voltage ripple of the HBSM capacitor is much smaller, only around 30 V. This result verifies the established theory of the inherently different energy variations of the hybrid MMC.

On the contrary, based on the proposed design method, the capacitances of the FBSM and the HBSM have $C_F = 1.92$ mF and $C_H = 0.53$ mF, respectively, and the corresponding waveforms are shown in Fig. 15. By simply reducing the HBSM capacitance, the overall capacitance is reduced by 36%. The voltage ripple of the HBSM capacitor is enlarged to the same level as the FBSM, which is 200 V. Meanwhile, the voltage balancing is still well maintained. The total harmonic distortion (THD) of the ac output voltage and the arm current are not significantly affected since all the capacitor voltage ripples are within 10%.

B. Experiments

A down-scale single-phase hybrid MMC prototype is built in the laboratory, as shown in Fig. 16. The experimental parameters are listed in Table IV. It includes two arms, namely the upper arm and lower arm, where each arm includes two FBSMs and two

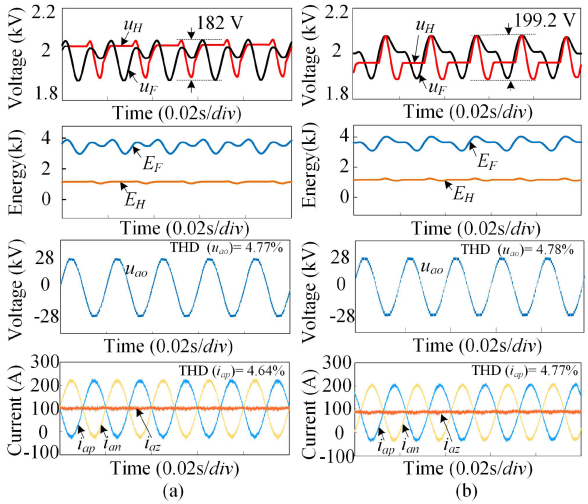

Fig. 15. Simulation result of hybrid MMC with the proposed method, i.e., $C_F = 1.92$ mF, $C_H = 0.53$ mF. (a) $\varphi = 0$. (b) $\varphi = -\pi/6$. The voltage ripples of the HBSM and FBSM capacitors are almost the same by the proposed method. (Top to Bottom: SM capacitor voltage, SM capacitor energy, AC output voltage, arm currents, and circulating current.)

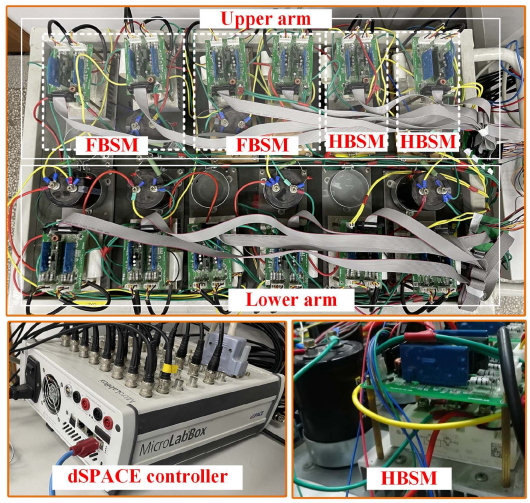

Fig. 16. Experimental setup of single-phase hybrid MMC.

HBSMs. Each HBSM consists of a capacitor, a half-bridge circuit, a driver board, and a heatsink. The MicroLabBox dSPACE is used to control the single-phase hybrid MMC.

Fig. 17 shows the experimental results of the hybrid MMC under $m = 1.6$, where the hybrid MMCs with different HBSM capacitances are compared. In Fig. 17(a), the capacitances of the FBSM and the HBSM are identical, which is $C_H = C_F = 2.2$ mF. The voltage ripple of the HBSM capacitor is smaller than that of the FBSM capacitor. In Fig. 17(b), the FBSM capacitance is sized as $C_F = 2.2$ mF but the HBSM capacitance is reduced to $C_H = 0.65$ mF by adopting the proposed method. The capacitor voltage ripple of the HBSM is enlarged but still within 10% of the nominal voltage. Besides, the THD of the hybrid MMC is not degraded by the proposed method, strengthening the advantage of the proposed capacitance design method.

TABLE IV
EXPERIMENTAL PARAMETERS

Parameters and symbols	Values and units
Nominal SM voltage U_C	50 V
Number of SMs N	4
Number of HBSMs N_H	2
Number of FBSMs N_F	2
DC bus voltage $U_{\rm dc}$	100 V
AC output voltage $U_{\rm ac}$	80 V
HBSM capacitance C_H	2.2 mF
FBSM capacitance C_F	0.65 mF
Arm inductance L_s	3.3 mH
Load resistance R	10 Ω

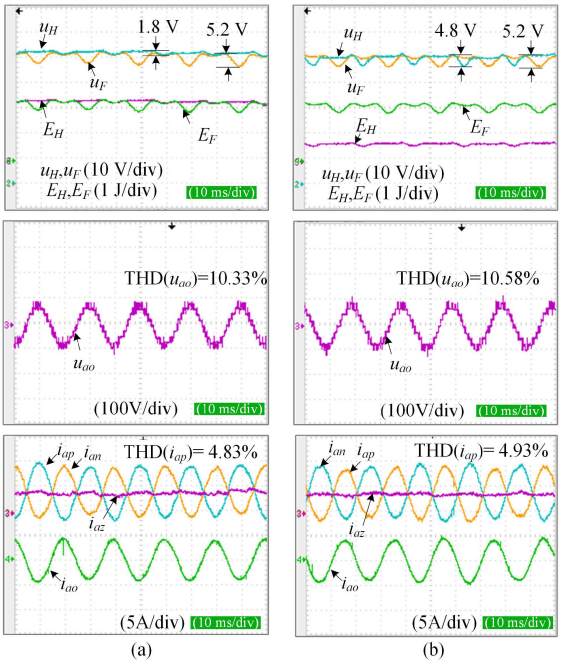

Fig. 17. Experimental results of the hybrid MMC: (a) Unified capacitance with $C_F = C_H = 2.2$ mF, the voltage ripple of the HBSM capacitor is much smaller than that of the FBSM capacitor. (b) Proposed method with $C_F = 2.2$ mF and $C_H = 0.65$ mF, the total capacitance is reduced by 36%, and the voltage ripple of the HBSM capacitor is increased but still limited within 10%.

VI. CONCLUSION

This article proposes a hybrid MMC working under the boost ac mode with reduced capacitance, which has great potential of being applied to the distribution networks. Apart from directly connecting to ac grid without bulk line transformers by the boost ac mode, the proposed hybrid MMC has additional benefits in terms of reducing capacitance and better efficiency. Based on the comprehensive evaluation in this article, the total capacitance of the hybrid MMC can be reduced by at least 36% compared with the existing concept. Although the capacitance reduction is similar to the FB-MMC, the proposed concept is able to reduce 15%–25% power losses and has less hardware.

To achieve this new concept, this article has three theoretical contributions. First, the hybridization ratio of the hybrid MMC is revisited. A more general principle of hybridization ratio selection is established considering dc fault blocking, voltage balancing, and negative output capability. Next, an improved piecewise approach is proposed to estimate the uneven and nonlinear energy variations of both FBSM and HBSM in a simple way, which avoids the complex calculation of the exact location of the converging point. Finally, this article fully utilizes the inherently different energy variations of the two types of SMs to design the capacitance separately. The proposed simple method helps to reduce capacitance without affecting the performance of the hybrid MMC.

REFERENCES

[1] M. A. Perez, S. Bernet, J. Rodriguez, S. Kouro, and R. Lizana, "Circuit topologies, modelling, control schemes and applications of modular multilevel converters," *IEEE Trans. Power Electron.*, vol. 30, no. 1, pp. 4–17, Jan. 2015.

[2] Z. Ke et al., "Capacitor voltage ripple estimation and optimal sizing of modular multi-level converters for variable-speed drives," *IEEE Trans. Power Electron.*, vol. 35, no. 11, pp. 12544–12554, Nov. 2020.

[3] A. Nami, J. Liang, F. Dijkhuizen, and G. D. Demetriades, "Modular multilevel converters for HVDC applications: Review on converter cells and functionalities," *IEEE Trans. Power Electron.*, vol. 30, no. 1, pp. 18–36, Jan. 2015.

[4] J. Zhang, X. Hu, S. Xu, Y. Zhang, and Z. Chen, "Fault diagnosis and monitoring of modular multilevel converter with fast response of voltage sensors," *IEEE Trans. Ind. Electron.*, vol. 67, no. 6, pp. 5071–5080, Jun. 2020.

[5] J. Peralta, H. Saad, S. Dennetiere, J. Mahseredjian, and S. Nguefeu, "Detailed and Averaged Models for a 401-Level MMC–HVDC System," *IEEE Trans. Power Del.*, vol. 27, no. 3, pp. 1501–1508, Jul. 2012.

[6] M. Lu, J. Hu, R. Zeng, W. Li, and L. Lin, "Imbalance mechanism and balanced control of capacitor voltage for a hybrid modular multilevel converter," *IEEE Trans. Power Electron.*, vol. 33, no. 7, pp. 5686–5696, Jul. 2018.

[7] J. Hu, M. Xiang, L. Lin, M. Lu, J. Zhu, and Z. He, "Improved design and control of FBSM MMC with boosted ac voltage and reduced dc capacitance," *IEEE Trans. Ind. Electron.*, vol. 65, no. 3, pp. 1919–1930, Mar. 2018.

[8] R. Zeng, L. Xu, L. Yao, and B. W. Williams, "Design and operation of a hybrid modular multilevel converter," *IEEE Trans. Power Electron.*, vol. 30, no. 3, pp. 1137–1146, Mar. 2015.

[9] M. Chen, S.-F. Chou, F. Blaabjerg, and P. Davari, "Overview of power electronic converter topologies enabling large-scale hydrogen production via water electrolysis," *Appl. Sci.*, vol. 12, no. 4, Feb. 2022, Art. no. 1906.

[10] T. Nakanishi and J.-I. Itoh, "High power density design for a modular multilevel converter with an H-bridge cell based on a volume evaluation of each component," *IEEE Trans. Power Electron.*, vol. 33, no. 3, pp. 1967–1984, Mar. 2018.

[11] L. Camurca, T. Pereira, F. Hoffmann, and M. Liserre, "Analysis, limitations, and opportunities of modular multilevel converter-based architectures in fast charging stations infrastructures," *IEEE Trans. Power Electron.*, vol. 37, no. 9, pp. 10747–10760, Sep. 2022.

[12] P. D. Judge, G. Chaffey, M. M. C. Merlin, P. R. Clemow, and T. C. Green, "Dimensioning and modulation index selection for the hybrid modular multilevel converter," *IEEE Trans. Power Electron.*, vol. 33, no. 5, pp. 3837–3851, May 2018.

[13] J.-H. Lee, J.-J. Jung, and S.-K. Sul, "Balancing of submodule capacitor voltage of hybrid modular multilevel converter under dc-bus voltage variation of HVDC system," *IEEE Trans. Power Electron.*, vol. 34, no. 11, pp. 10458–10470, Nov. 2019.

[14] Y. Dong, J. Tang, H. Yang, W. Li, and X. He, "Capacitor voltage balance control of hybrid modular multilevel converters with second- order circulating current injection," *IEEE J. Emerg. Sel. Topics Power Electron.*, vol. 7, no. 1, pp. 157–167, Mar. 2019.

[15] P. Hu, Z. He, R. Yin, J. Guo, M. J. Guerrero, and R. Teodorescu, "Analysis and optimization of hybrid modular multilevel converters under overmodulation conditions," *Int. J. Electric. Power Energy Syst.*, vol. 116, Mar. 2020, Art. no. 105578.

[16] J. Zhang, Y. Zhang, F. Deng, and Z. Din, "Overmodulation operation of hybrid modular multilevel converter with reduced energy storage requirement," *IEEE J. Emerg. Sel. Topics Power Electron.*, vol. 10, no. 3, pp. 2946–2958, Jun. 2022.

[17] J. Xu et al., "Dual harmonic injection for reducing the submodule capacitor voltage ripples of hybrid MMC," *IEEE J. Emerg. Sel. Topics Power Electron.*, vol. 9, no. 3, pp. 3622–3633, Jun. 2021.
[18] C. Zhao et al., "Energy storage requirement optimization of hybrid modular multilevel converter with circulating current injection," *IEEE Trans. Ind. Electron.*, vol. 66, no. 9, pp. 6637–6648, Sep. 2019.
[19] Z. Li et al., "Reduction in submodule capacitance in FB- and HYB-MMCs with variable dc voltages," *IEEE Trans. Ind. Electron.*, vol. 70, no. 6, pp. 5808–5818, Jun. 2023.
[20] N. P. Rao and A. Shukla, "Analysis of capacitor voltage unbalance in hybrid MMC and its novel operation with reduced submodule capacitance," *IEEE J. Emerg. Sel. Topics Power Electron.*, vol. 10, no. 6, pp. 7271–7284, Dec. 2022.
[21] L. Lin, Y. Lin, C. Xu, and Y. Chen, "Comprehensive analysis of capacitor voltage fluctuation and capacitance design for submodules in hybrid modular multilevel converter with boosted modulation index," *IEEE J. Emerg. Sel. Topics Power Electron.*, vol. 7, no. 4, pp. 2369–2383, Dec. 2019.
[22] K. Ilves, S. Norrga, L. Harnefors, and H.-P. Nee, "On energy storage requirements in modular multilevel converters," *IEEE Trans. Power Electron.*, vol. 29, no. 1, pp. 77–88, Jan. 2014.
[23] Z. Li, P. Wang, Z. Chu, H. Zhu, Y. Luo, and Y. Li, "An inner current suppressing method for modular multilevel converters," *IEEE Trans. Power Electron.*, vol. 28, no. 11, pp. 4873–4879, Nov. 2013.
[24] S. Milovanović and D. Dujić, "Comprehensive comparison of modular multilevel converter internal energy balancing methods," *IEEE Trans. Power Electron.*, vol. 36, no. 8, pp. 8962–8977, Aug. 2021.
[25] Y. Zhang, J. Zhang, and F. Deng, "Improved CPS-PWM approach for over-modulation operations of hybrid modular multilevel converter," *IEEE J. Emerg. Sel. Topics Power Electron.*, vol. 10, no. 5, pp. 5933–5943, Oct. 2022.
[26] Y. Zhang, "System-level power loss evaluation of modular multilevel converters," in *Proc. IEEE Energy Convers. Congr. Expo.*, 2019, pp. 6797–6804.
[27] Y. Zhang, H. Wang, Z. Wang, F. Blaabjerg, and M. Saeedifard, "Mission profile-based system-level reliability prediction method for modular multilevel converters," *IEEE Trans. Power Electron.*, vol. 35, no. 7, pp. 6916–6930, Jul. 2020.

Yaqian Zhang (Member, IEEE) received the B.S. degree from the University of Electronic Science and Technology of China, Chengdu, China, in 2016, and the Ph.D. degree from Southeast University, Nanjing, China, in 2023, both in electrical engineering.

From 2021 to 2022, she was a Visiting Ph.D. Student with the Department of Energy Technology, Aalborg University, Aalborg, Denmark. She is currently a Lecturer with Southeast University. Her research focuses on high-voltage power electronic converters, including the modular multilevel converter and the solid-state transformer.

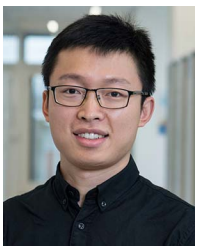

Yi Zhang (Member, IEEE) received the B.S. and M.S. degrees from the Harbin Institute of Technology, Harbin, China, in 2014 and 2016, respectively, and the Ph.D. degree from Aalborg University, Aalborg, Denmark, in 2020, all in electrical engineering.

In 2018, he was a Visiting Scholar with the Georgia Institute of Technology, Atlanta, GA, USA. From 2020 to 2023, he was affiliated with multiple institutions as a Postdoctoral Researcher with the support of the Danish Research Council for Independent Research, including RWTH-Aachen University, Aachen, Germany, the Swiss Federal Institute of Technology Lausanne, Lausanne, Switzerland, and the Massachusetts Institute of Technology, Cambridge, MA, USA. He is currently an Assistant Professor with Aalborg University. His research interests include the reliability and optimization of power electronics.

Dr. Zhang was the recipient of the First Place Prize Paper Award of the IEEE TRANSACTIONS ON POWER ELECTRONICS, in 2021, and was the IEEE Power Electronics Society Ph.D. Thesis Award Winner, in 2020.

Jianzhong Zhang (Senior Member, IEEE) received the M.Sc. and Ph.D. degrees in electrical engineering from the Department of Electrical Engineering, Southeast University, Nanjing, China, in 2005 and 2008, respectively.

From 2006 to 2007, he was a Visiting Scholar with the Department of Energy Technology, Aalborg University, Aalborg, Denmark. Since 2008, he has been with Southeast University, where he is currently a Research Professor with the School of Electrical Engineering. He was a Visiting Professor with the Worcester Polytechnic Institute, Worcester, MA, USA, and the University of British Columbia, Vancouver, BC, Canada, in July 2012 and August 2017, respectively. His research interests include power electronics, electrical machines, and renewable power generation.

Dr. Zhang was the recipient of the Institution Premium Award at the Institutions of Engineering and Technology, U.K.

Fujin Deng (Senior Member, IEEE) received the B.Eng. degree in electrical engineering from the China University of Mining and Technology, Beijing, China, in 2005, the M.Sc. degree in electrical engineering from Shanghai Jiao Tong University, Shanghai, China, in 2008, and the Ph.D. degree in energy technology from the Department of Energy Technology, Aalborg University, Aalborg, Denmark, in 2012.

In 2017, he was a Professor with the School of Electrical Engineering, Southeast University, Nanjing, China. From 2013 to 2015 and from 2015 to 2017, he was a Postdoctoral Researcher and an Assistant Professor, respectively, with the Department of Energy Technology, Aalborg University. His main research interests include wind power generation, multilevel converters, high-voltage direct-current technology, dc grid, and offshore wind farm-power systems dynamics.

Frede Blaabjerg (Fellow, IEEE) received the Ph.D. degree in electrical engineering from Aalborg University, Aalborg, Denmark, in 1995.

From 1987 to 1988, he was with ABBScandia, Randers, Denmark. He was an Assistant Professor in 1992, an Associate Professor in 1996, and a Full Professor of Power Electronics and Drives in 1998. In 2017, he was a Villum Investigator. He is honoris causa with University Politehnica Timisoara, Timisoara, Romania, and Tallinn Technical University, Tallinn, Estonia. His current research interests include power electronics and its applications, such as in wind turbines, PV systems, reliability, harmonics, and adjustable speed drives.

Dr. Blaabjerg was the recipient of 32 IEEE Prize Paper Awards, the IEEE PELS Distinguished Service Award in 2009, the EPE-PEMC Council Award in 2010, the IEEE William E. Newell Power Electronics Award in 2014, the Villum Kann Rasmussen Research Award in 2014, the Global Energy Prize in 2019, and the 2020 IEEE Edison Medal. From 2006 to 2012, he was the Editor-in-Chief of the IEEE TRANSACTIONS ON POWER ELECTRONICS. He was a Distinguished Lecturer of the IEEE Power Electronics Society from 2005 to 2007, and for the IEEE Industry Applications Society from 2010 to 2011, as well as from 2017 to 2018. He was the President of the IEEE Power Electronics Society, from 2019 to 2020. He is the Vice-President of the Danish Academy of Technical Sciences. He was nominated from 2014 to 2019 by Thomson Reuters to be among the 250 most cited researchers in engineering in the world.